Int. J. Heat Mass Transfer. Vol. 35, No. 5, pp. 1155–1167, 1992
Printed in Great Britain

0017–9310/92 $5.00 + 0.00

The transient thermal response of a glass-fiber insulation slab with hygroscopic effects

Y.-X. TAO, R. W. BESANT and K. S. REZKALLAH
Department of Mechanical Engineering, University of Saskatchewan, Saskatoon, Saskatchewan S7N 0W0, Canada

(*Received* 1 *March* 1991 *and in final form* 3 *May* 1991)

Abstract—The Brunauer–Emmett–Teller (BET) equation, representing adsorption isotherms, is used in a one-dimensional, transient vapor-diffusion model for heat and moisture transport in a typical, medium-dry density glass-fiber insulation slab to account for the hygroscopic effects (water vapor adsorption, desorption, and capillary condensation). The correction to the latent enthalpy of phase change, used in the energy equation, is derived from empirical desorption isotherms. The results obtained, for two types of boundary conditions (a closed system and an open system), show that the effects of hygroscopicity on the transient temperature distribution are significant for a slab with one boundary open to moist air. The sensitivity of hygroscopicity on the transient heat and mass transfer behavior can be depicted by a transition Fourier number, which is proportional to the adsorption capacity of the glass-fiber slab and increases as the cold side temperature and ambient relative humidity increase. Given the uncertainty in the adsorption properties of fiber-glass and experimental data, the agreement between the model and measured data is reasonable.

1. INTRODUCTION

HEAT AND moisture transport through insulation materials has been of considerable interest among researchers, not only because of its practical significance in energy conservation for building and refrigerated space envelopes, but also because of the physical complexity of problems in various transient circumstances. In practice, the consequences of the failure of vapor retarders in air-tight structures due to installation problems (among other factors) are well known in the design and consulting communities [1]. This failure of vapor retarders may, depending on temperature and air exfiltration rates, result in significant water and/or frost accumulation in building envelopes. In order to understand the physics of the transport processes in those situations, studies have been conducted analytically and numerically [2–4] along with the experimental efforts [5–8]. For applied temperature ranges above the freezing point, the investigation has been conducted to include condensation effects [9, 10] and air infiltration/exfiltration effects [11]. It has been shown that the additional, steady-state heat loss, due to condensation of water in an insulation slab under a thermal gradient, is negligible if the mass transport process in the slab is dominated by vapor molecular diffusion (i.e. $Pe = 0$) and the Lewis number ($\alpha^*_{0,\text{eff}}/D^*_{v,\text{eff}}$) is small [9]. This conclusion is supported by an early experimental study by Kumaran [7] in which a glass-fiber insulation slab, after being open to a moist air at 97% relative humidity for a long time, showed no significant increase in heat flux as compared to a dry slab. It has also been reported by Wijeysundera *et al.* [8], for an insulation slab with its impermeable cold side (an ideal vapor 'barrier' applied) and the warm side open to a forced convective moist air at a relative humidity of less than 80%, the heat loss is almost the same as if the slab is dry. However, when the cold side of the insulation slab is subject to a temperature below the triple point of water, condensed water may exist as frost which both alters the temperature distribution and increases the effective thermal conductivity of the slab. A numerical study [12] shows that condensation and frosting in a typical glass-fiber slab will result in a 10–30% increase in heat flux at the quasi-steady-state when the ambient air relative humidity is above 60%.

In all the numerical studies mentioned above, the hygroscopicity of the glass-fiber insulation was not considered in the models. Condensation, or frosting, is assumed to occur when the local vapor density reaches its saturation value, i.e. no water vapor adsorption is considered. Mitalas and Kumaran [13] made an estimate of the hygroscopic effects for a glass-fiber slab which was in a closed system; their test facility contained a fixed quantity of water and vapor in a sealed cell and was not exposed to ambient moist air. They concluded that the hygroscopic effects on the thermal performance was negligible when this wrapped slab was subject to a temperature difference in their heat flow measurement apparatus. However, previous experimental work [14] shows that, when an initially oven-dried glass-fiber slab has one side open to moist air and is subjected to a large temperature difference across the slab, the measured internal slab temperatures and heat flux from the cold surface are higher than those predicted using a model that excludes the hygroscopicity effects. It was found that only for a slab, that was initially wetted, were the

NOMENCLATURE

Bi	Biot number, $h_a L/k^*_{eff}$
Bi_m	mass transfer Biot number, $h_m L/D^*_{v,eff}$
C	empirical constant in equation (12)
c_p	heat capacity at constant pressure
D_{eff}	dimensionless diffusivity, $D^*_{v,eff}/\alpha^*_{0,eff}$
$D^*_{v,eff}$	effective vapor diffusivity [$m^2\ s^{-1}$]
Fo	Fourier number, $\alpha^*_{0,eff} t^*/L^2$
h	enthalpy of phase change
h^*_{fg}	enthalpy of vaporization [$J\ kg^{-1}$]
h^*_{sg}	enthalpy of sublimation [$J\ kg^{-1}$]
k	thermal conductivity
L	characteristic length of the slab [m]
$\dot{m}$	rate of phase change
p	pressure
Q'	heat-flux ratio defined in equation (30)
R^*_a	air gas constant [$J\ kg^{-1}\ K^{-1}$]
R^*_v	water vapor gas constant [$J\ kg^{-1}\ K^{-1}$]
t	time
T	temperature
ΔT^*	reference temperature difference, $T^*_a - T^*_c$ [K]
W	water content per unit dry mass
W_m	empirical constant in equation (12)
z	coordinate axis.

Greek symbols

$\alpha^*_{0,eff}$	effective thermal diffusivity [$m^2\ s^{-1}$]
ε	volume fraction
ϕ	relative humidity
ρ	density
τ	tortuosity.

Subscripts

a	air
c	cold
ref	reference
s	saturated
t	total
tr	transition
v	vapor phase
β	liquid or ice phase
γ	gas phase which consists of air and water vapor
σ	solid phase
0	initial; reference for non-dimensional scales (Table 1).

Superscripts

′	ratio
*	dimensional.

measured temperature and heat flux close to the prediction. These observations lead to a speculation that the hygroscopicity in fiber-glass insulation may have a strong effect on its transient thermal performance. This speculation must be justified through the understanding of the physical phenomena involved in hygroscopic heat and mass transfer.

It is known that physical adsorption and capillary condensation are the main mechanisms of phase change during hygroscopic mass transfer in glass-fiber materials [6, 15]. The hygroscopicity (here we only deal with water vapor) for a material is traditionally characterized by empirical, equilibrium adsorption or desorption isotherms. These isotherms represent the amount of vapor adsorbed at thermodynamic equilibrium conditions as a function of the relative humidity of the moist air. The typical adsorption and desorption isotherm data for glass-fiber materials [5, 6] are shown in Fig. 1. It can be seen that, besides temperature and relative humidity, the capacity for adsorption strongly depends on the percentage and type of bonding materials used in making insulation boards and is also a function of the glass-fiber diameter (or specific surface area) and insulation bulk density. Applying this knowledge to a relatively thick insulation slab, subject to a thermal gradient and assuming local thermodynamic equilibrium, we can conclude that phase change occurs by adsorption or desorption even when the local relative humidity is less than 100%. For the local relative humidity between 90

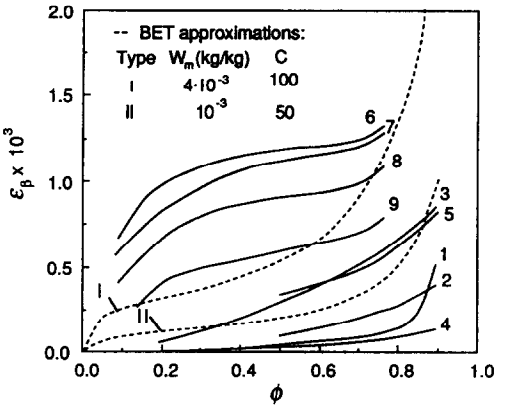

Test conditions for adsorption/desorption isotherms

Test	ρ_0 (kg/m³)	$\bar{d}$(μ m)	τ(%)	T(°C)	Ref.
1	100	6	0	50	[5]
2	70	5	9.7	"	"
3	121	12	11	"	"
4	20	6	5.7	"	"
5	100	6	12.8	"	"
6	101	11.6	10.7	10	[6]
7	"	"	"	20	"
8	"	"	"	30	"
9	"	"	"	40	"

ρ_0—dry density; $\bar{d}$—average fiber diameter;
τ—bonding percentage; T— temperature.

FIG. 1. Adsorption and desorption isotherms for different glass-fiber insulations. Also shown are BET approximations I and II.

and 100%, capillary condensation may occur depending on the local pore structure. Furthermore, phase change mass transfer is coupled with heat transfer during an adsorption process, i.e. the energy that equals the mass of adsorption multiplied by the enthalpy of adsorption is released, acting as a heat source. Since the enthalpy of adsorption is usually larger than the enthalpy of condensation, it is expected that the transient temperature field in the slab will be different from that in a non-hygroscopic glass-fiber slab. During a transient thermal response test, these hygroscopic effects are expected to be stronger for an initially dry sample that is subject to a large temperature difference across it.

In this study, we include the effects of hygroscopicity in solving for the temperature, vapor density, phase-change rate, and water/frost (defined as β-phase) volume fraction distributions for an initially dry glass-fiber insulation slab undergoing a transient process. The objective of this study is to investigate the sensitivity of the hygroscopic effects on these properties. To do so, we use the well-known BET approximation (Type II isotherm) [16] to represent the adsorption isotherms, as indicated in Fig. 1, which shows agreement with experimental data for low hygroscopicity effects in glass-fibers at higher temperature ranges and for other isotherms at low relative humidity ranges. Since no generalized mathematical form can account for all the factors influencing the hygroscopicity of glass-fiber insulations, using the two-parameter BET equation allows us to simplify the formulation but still keep the essence of hygroscopic sensitivity in coupling heat and mass transport. The enthalpy of adsorption is deduced from the isotherm data given by ref. [6] using thermodynamic relations. Calculations are performed for both a closed system and an open system with one side impermeable. The effects of the cold side temperature and ambient air relative humidity (for an open system) are discussed. The predicted temperature and heat flux are compared with the experimental data obtained using an apparatus reported earlier [14].

2. ANALYSIS

2.1. *One-dimensional, transient vapor diffusion*

The problem is formulated, as a one-dimensional, transient, simultaneous heat and mass transfer problem, using the local volume averaging technique [17], as shown in Fig. 2. Vapor diffusion is the mode for the moisture transport, and phase changes are caused by condensation, ablimation† and adsorption. The major assumptions are listed in Appendix A and are discussed in ref. [12].

The dimensionless forms of the governing differential equations are

†Ablimation means a substance changing from its vapor phase to a solid phase. The word was used by P. W. B. Harrison [18].

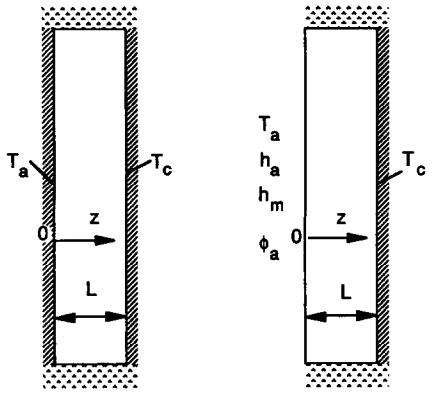

FIG. 2. Transient, one-dimensional condensation, frosting and adsorption in an insulation slab for two systems: (a) closed, (b) open.

β-phase continuity equation

$$\frac{\partial \varepsilon_\beta}{\partial t} + \frac{\dot{m}}{P_1} = 0 \tag{1}$$

gas diffusion equation

$$\frac{\partial(\varepsilon_\gamma \rho_v)}{\partial t} - \dot{m} = \frac{\partial}{\partial z}\left(D_{\text{eff}} \frac{\partial \rho_v}{\partial z}\right) \tag{2}$$

energy equation

$$\rho c_p \frac{\partial T}{\partial t} + \dot{m} P_2 h' = \frac{\partial}{\partial z}\left(k_{\text{eff}} \frac{\partial T}{\partial z}\right) \tag{3}$$

where the symbols are listed in the Nomenclature, the dimensionless variables and parameters are defined in Table 1, and h' is the ratio of the heat of adsorption to the heat of condensation (or heat of sublimation). The algebraic equations of constraint are

volumetric constraint

$$\varepsilon_\sigma + \varepsilon_\beta + \varepsilon_\gamma = 1 \tag{4}$$

thermodynamic relations

$$p_a = p_t - p_v \tag{5}$$

$$p_a = P_3 \rho_a T \tag{6}$$

$$p_v = P_4 \rho_v T \tag{7}$$

and for saturation conditions

$$p_v = \exp\left[-P_5\left(\frac{1}{T} - \frac{1}{T_{\text{ref}}}\right)\right] \tag{8}$$

where

$$\rho = \varepsilon_\sigma \rho_\sigma + \varepsilon_\beta \rho_\beta + \varepsilon_\gamma(\rho_v + \rho_a) \tag{9}$$

$$c_p = \frac{\varepsilon_\sigma \rho_\sigma c_\sigma + \varepsilon_\beta \rho_\beta c_\beta + \varepsilon_\gamma(c_v \rho_v + c_a \rho_a)}{\rho} \tag{10}$$

$$k_{\text{eff}} = \varepsilon_\sigma k_\sigma + \varepsilon_\beta k_\beta + \varepsilon_\gamma \frac{k_v \rho_v + k_a \rho_a}{\rho_v + \rho_a}. \tag{11}$$

Table 1(a). Dimensionless variables

ρ	c_p	T	ρ_i	k_i	p_i	z	c_i	k_{eff}	t	$\dot{m}$
$\frac{\rho^*}{\rho_0^*}$	$\frac{c_p^*}{c_0^*}$	$\frac{T^*}{\Delta T^*}$	$\frac{\rho_i^*}{\rho_0^*}$	$\frac{k_i^*}{k_{0,\text{eff}}^*}$	$\frac{p_i^*}{p_{v,0}^*}$	$\frac{z^*}{L}$	$\frac{c_i^*}{c_0^*}$	$\frac{k_{\text{eff}}^*}{k_{0,\text{eff}}^*}$	$\frac{t^*}{L^2/\alpha_{0,\text{eff}}^*}$	$\frac{\dot{m}^*}{\rho_0^*\alpha_{0,\text{eff}}^*/L^2}$

Table 1(b). Dimensionless parameters

	P_1		P_2				P_5	
D_{eff}	Liquid	Ice	Liquid	Ice	P_3	P_4	Liquid	Ice
$\frac{D_{v,\text{eff}}^*}{\alpha_{0,\text{eff}}^*}$	$\frac{\rho_\beta^*}{\rho_0^*}$	$\frac{\rho_{\beta,\text{ice}}^*}{\rho_0^*}$	$\frac{h_{\text{fg}}^*}{c_0^*\Delta T^*}$	$\frac{h_{\text{sg}}^*}{c_0^*\Delta T^*}$	$\frac{\Delta T^* R_0^* \rho_0}{p_{v,0}^*}$	$\frac{\Delta T^* R_0^* \rho_0}{p_{v,0}^*}$	$\frac{h_{\text{fg}}^*}{R_v^*\Delta T^*}$	$\frac{h_{\text{sg}}^*}{R_v^*\Delta T^*}$

In the above formulation, the unknown variables are T, ρ_v, ρ_a, ε_β, ε_γ, $\dot{m}$, p_a, and p_v while all the transport and thermophysical properties for the individual phases are known from empirical data. Equations (1)–(8) can then be used to solve for these eight unknowns if the phase changes are due to condensation and frosting. However, if the adsorption process occurs, equation (8) can no longer be used to describe the local vapor density when the local relative humidity, ϕ, is less than 100%. An alternative equation characterizing the hygroscopicity of the material is needed.

2.2. *The BET approximation (Type II isotherms)*

The majority of physical adsorption isotherms reported in the literature can be grouped into five classes—the five types, I–V, of the so-called BET classification [15]. In Fig. 1, the experimental adsorption isotherms reported by Langlais *et al.* [5] seem to fit the Type II isotherms using the following BET approximation:

$$\frac{W}{W_m} = \frac{C\phi}{[1-\phi][1+(C-1)\phi]} \tag{12}$$

where W is the mass of vapor adsorbed (adsorbate) per mass of the dry sample (adsorbent), and W_m and C are empirical constants which are generally functions of temperature and solid/gas properties. The major assumptions of the BET model are that all the adsorption sites on the surface are energetically identical and that there is no lateral interaction between the neighboring adsorbate molecules. The model allows for multi-molecule-layer adsorption [15]. The Type II isotherms are, in the majority of cases, used to describe the physical adsorption by non-porous solids. This is consistent with the structural nature of most glass-fiber insulation slabs, which usually have very high porosity (>90%) and large pore sizes. This makes a tortuosity (for water diffusion within the pores) very close to unity so that the interaction, between the vapor and the fiber matrix of the insulation, is essentially the same as that between the vapor and the glass surface coated with the bonding material. For the desorption curves reported by Pierce and Benner [6], tests 6–9 in Fig. 1, it is not very clear that these isotherms are Type II, due to the lack of data for the relative humidity above 0.8. It is suspected that hysteresis may be partly responsible for the curves deviating from Type II isotherms. In that case, Type IV may be the best fit [16], although in ref. [6], a purely empirical polynomial correlation is reported. Since the available data for higher relative humidities and lower temperatures are limited and our focus here is on the parametric study of hygroscopicity on the transient thermal behavior for any type of glass-fiber insulation, we choose the established BET equation (12), as a supplementary equation to the formulation by defining

$$W = \varepsilon_\beta \rho_\beta + \varepsilon_\gamma(\rho_v + \rho_a). \tag{13}$$

In this treatment, the influence of temperature on the hygroscopicity is included in the local relative humidity, ϕ. The BET equation, then, simply gives a relation between ε_β and ϕ for given W_m and C. Two sets of W_m and C are selected, as indicated in Fig. 1, in separate calculations. Approximation I ($W_m = 4\times10^{-3}$, $C = 100$) stands for the glass-fibers with a higher adsorption capacity, which corresponds to an insulation having a higher percentage of the bonding material, or at a relatively lower temperature range, than that represented by Approximation II ($W_m = 1\times10^{-3}$, $C = 50$). Further information on the BET equation and the physics of W_m and C can be found in ref. [16].

2.3. *Enthalpy of adsorption*

Similar to the adsorption/desorption isotherm data, the enthalpy of adsorption is usually determined experimentally. One of the methods is to deduce the enthalpy of adsorption from the isotherm data [16]. This enthalpy of adsorption is called the isosteric enthalpy of adsorption, h_{ad}^* (J kg^{-1}). From thermodynamics, it is known that h_{ad}^* obeys the Clapeyron equation (8)

$$\left(\frac{\partial \ln p_v^*}{\partial T^*}\right)_W = \frac{h_{\text{ad}}^*}{R_v^* T^{*2}}$$

or

$$(\ln p_v^*)_W = -\frac{h_{\text{ad}}^*}{R_v^* T^*} + f_1(W). \tag{14}$$

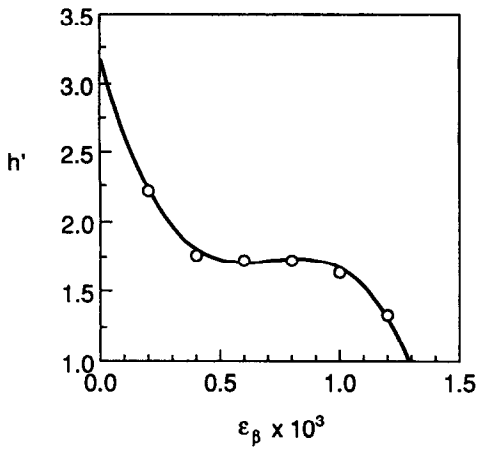

FIG. 3. The ratio of the isosteric enthalpy of adsorption to the enthalpy of condensation for a typical fibrous insulation [6].

For condensation, without hygroscopic effects, we have

$$\ln p_s^* = -\frac{h_{fg}^*}{R_v^* T^*} + \text{constant}. \tag{15}$$

Then, combining equations (14) and (15) yields

$$(\ln p_v^*)_W = \left.\frac{h_{ad}^*}{h_{fg}^*}\right|_W \ln p_s^* + f_2(W). \tag{16}$$

From the isotherms, the relation between p_v^* ($=\phi p_s^*$) and p_s^* can be found for a given W. The slope on a $\ln p_v^*$ vs $\ln p_s^*$ plot is then h_{ad}^*/h_{fg}^*. In Fig. 3, the enthalpy of adsorption is, considering equation (13), shown in the following form:

$$h' = \frac{h_{ad}^*}{h_{fg}^*} = f(\varepsilon_\beta) \tag{17}$$

which is correlated using a polynomial in the calculations. It can be seen from Fig. 3 that after ε_β exceeds 1.3×10^{-3}, h' approaches unity and bulk condensation takes place. This transition β-phase volume fraction, which is much larger than that used in refs. [9–12], seems more consistent with the data when distinguishing between the adsorption and bulk-phase-change processes.

2.4. *Boundary conditions*

Two cases are considered to investigate the significance of transient hygroscopic effects with a step change in the cold boundary temperature (see Fig. 2): (a) both boundaries are impermeable to water vapor flow (a closed system); (b) one boundary is impermeable and the warm boundary is open to a moist air flow (an open system). Case (a) is typical for any thermal performance test of an insulation such as for the measurement of thermal conductivity [7, 8]. Case (b) is also typical to some of the practical field conditions and was studied previously [12, 14]. The boundary conditions for those cases are

Case (a)

$$T(z=0,t) = T_a \tag{18}$$

$$\frac{\partial \rho_v(z=0,t)}{\partial z} = 0 \tag{19}$$

$$T(z=1,t) = T_c \tag{20}$$

$$\frac{\partial \rho_v(z=1,t)}{\partial z} = 0. \tag{21}$$

If ρ_v at $z = 0$ or 1 reaches ρ_s, the boundary conditions (19) and (21) are replaced by $\rho_v = \rho_s$ using the saturation condition, equation (8).

Case (b)

$$\frac{\partial T(z=0,t)}{\partial z} = -Bi[T_a - T(z=0,t)] \tag{22}$$

$$\frac{\partial \rho_v(z=0,t)}{\partial z} = -Bi_m[\rho_a - \rho_v(z=0,t)] \tag{23}$$

$$T(z=1,t) = T_c \tag{24}$$

$$\frac{\partial \rho_v(z=1,t)}{\partial z} = 0. \tag{25}$$

Again, $\rho_v = \rho_s$, using equation (8), will replace equation (25) when $\rho_v(z=1,t)$ reaches the saturated value.

The initial conditions for both cases are

$$T(z, t=0) = T_0 \tag{26}$$

$$\rho_v(z, t=0) = \phi_0 \rho_s[T(z, t=0)] \tag{27}$$

$$\varepsilon_\beta(z, t=0) = \varepsilon_{\beta 0}(z). \tag{28}$$

The finite difference forms of equations (1)–(3) are derived using the implicit scheme with the backward difference for the time derivative. The central difference form is used for internal nodes and the backward, or forward difference, used for the boundary nodes. The computational procedure, including hygroscopic effects, is that, at each time step, the computed vapor density distribution is compared with the saturation vapor density calculated from equation (8) at the corresponding temperature. If the actual vapor density in a region is less than the saturation density, mass transfer is considered to be still in the adsorptive stage. Equations (1)–(7), (12) and (17) are used. If the local relative humidity, $\phi = p_v/p_s$, is greater than or equal to 0.95, bulk condensation, or frosting, is assumed to start for the next time step. The relative humidity 0.95 is chosen based on the assumption that above this relative humidity, the phase change is at a capillary condensation state. Strictly, the capillary effects can be included by using the Kelvin equation; however, according to ref. [10], the reduction of vapor partial pressure due to capillary condensation is negligible for glass-fiber insulations, i.e. in the range of $\phi = 0.95$–1.0, it is sufficient to use the Clapeyron equation, equations (8), to find the vapor partial pressure. For cases with no hygroscopic effects, phase changes are considered to occur only when the local

Table 2. Physical data and experimental conditions

ρ_0^*	kg m^{-3}	67.2
c_0^*	J kg^{-1} K^{-1}	840.7
D	m^2 s^{-1}	2.39×10^{-5}
$k_{0,\mathrm{eff}}^*$	W m^{-1} K^{-1}	0.037
L	m	0.09525
ε_σ		0.065
T_0^*	K	294
T_a^*	K	294
T_c^*	K	252
T_{ref}^*	K	273.16
h_{fg}^*	J kg^{-1}	2.5×10^6
h_{sg}^*	J kg^{-1}	2.8×10^6
ρ_σ^*	kg m^{-3}	2600
c_σ^*	J kg^{-1} K^{-1}	836.8
k_σ^*	W m^{-1} K^{-1}	0.243
ρ_β^*	kg m^{-3}	999.87
c_β^*	K kg^{-1} K^{-1}	4200
k_β^*	W m^{-1} K^{-1}	0.57
ρ_β^* (ice)	kg m^{-3}	917.0
c_β^* (ice)	J kg^{-1} K^{-1}	1924
k_β^* (ice)	W m^{-1} K^{-1}	2.22
c_v^*	J kg^{-1} K^{-1}	1882
k_v^*	W m^{-1} K^{-1}	0.0247
R_v^*	J kg^{-1} K^{-1}	461.89
k_a^*	W m^{-1} K^{-1}	0.0227
c_a^*	J kg^{-1} K^{-1}	1005
h_a^*	W m^{-2} K^{-1}	16.0

relative humidity reaches unity for an initially dry slab; therefore, a dry period initially appears [12]. In the calculations for this period, $\dot{m}$ in equations (1)–(3) is set to zero and ρ_v is basically determined from equation (3). After vapor diffusion causes an increase in the vapor density up to a saturation value, vapor condenses; equations (7) and (8) are then used to calculate ρ_v; equation (3) is used for solving $\dot{m}$; and ε_β and T are solved from equations (1) and (3), respectively [12]. For the purpose of discussion in the following section, the formulation that excludes the hygroscopic phenomena will be referred to as the bulk-phase-change model and the one including the hygroscopicity effect will be called the adsorption model. In all the calculations, we choose $\Delta t/(\Delta z)^2 \leqslant 2.25$ with the grid size $\Delta z = 0.05$, considering the balance between the accuracy, economy of computing time, and stability requirement. For each time step, the difference equations are solved using the under-relaxation iteration scheme. The solution is considered to be converged when the deviation of any variable from the last iterated value is within 10^{-3}%. The physical properties used in modeling are summarized in Table 2. These data are chosen in order to compare with the experimental results using an apparatus, reported earlier [14], which is briefly described in Appendix B.

3. RESULTS AND DISCUSSION

In the following, we first present the numerical results to examine the physics involved in transient, hygroscopic mass transfer under a thermal gradient. Then we compare the results obtained from the adsorption model and the bulk-phase-change model with the experimental results. Finally, we discuss the time scale (the transition Fourier number) characterizing a hygroscopic process.

3.1. *Moisture/frost accumulation under hygroscopic mass transfer for an open system*

In Fig. 4, the spatial distribution of the vapor density, temperature, rate of phase change, liquid/frost volume fraction and local relative humidity for an open system are shown at various times. In this example, the BET I approximation is applied, while the ambient air relative humidity is 0.97. Since the slab is initially dry ($\phi_0 = 10^{-7}$), the difference between the ambient vapor concentration and that inside provides a potential for an inward vapor diffusion, which causes an increase in ρ_v (Fig. 4(a)) and ε_β (Fig. 4(c)). However, this inward diffusion flux is attenuated by local adsorption. As can be seen in Fig. 4(a) at point A, the diffusion front only reaches $z = 0.53$ at $Fo = 0.035$. If, on the other hand, the fibers are non-hygroscopic, this diffusion front would have reached through the insulation slab ($z = 1$) within a very short time period (for example, $Fo < 0.005$ [12]), while in Fig. 4, this transition Fourier number is about 0.248. As a result of this delay in the diffusion front, the adsorbed vapor is mostly accumulated near the warm side of the slab for the Fo values shown. When the slab is initially subject to a step change in the cold side temperature, the energy released during adsorption contributes to a significant increase in temperature ($Fo = 0.035$, Fig. 4(b)). The magnitude of this temperature increase depends on the capacity of hygroscopicity, which is relatively high in this example. Also shown in Fig. 4(d), the maximum rate of adsorption, $\dot{m}$, is near the diffusion front at $Fo = 0.035$ due to a sharp change in the diffusion flux.

Within the range of Fo studied in Fig. 4, the local relative humidity never exceeds 0.95 as shown in Fig. 4(e). The whole process is essentially adsorption under vapor diffusion. This is not true if the insulation slab has the hygroscopicity obeying the BET II approximation. As shown in Fig. 5, where the same initial and boundary conditions are applied, $\phi(z = 1)$ has reached 1.0 at $Fo = 0.117$. The profiles in the slab indicate that there can be four different phase change regions existing at the same time for $Fo > 0.117$. For example, at $Fo = 0.489$, desorption or evaporation takes place near the warm side of the slab ($z < 0.25$) where $\dot{m}$ becomes positive (Fig. 5(d)), while adsorption still occurs in the middle portion of the slab, and for $z > 0.65$ condensation ($T > T_{\mathrm{ref}}$), or ablimation ($T \leqslant T_{\mathrm{ref}}$), happens. In this case, desorption or evaporation, near the warm side, is observed because ϕ_a is near 1.0. For cases with $\phi_a < 0.8$, this region is still in adsorption (see the broken line in Fig. 5(d)). The desorption and evaporation cause a decrease in ε_β as Fo increases (see Fig. 5(c) for $z < 0.25$ and $Fo = 0.489$), and the maximum accumulation of water

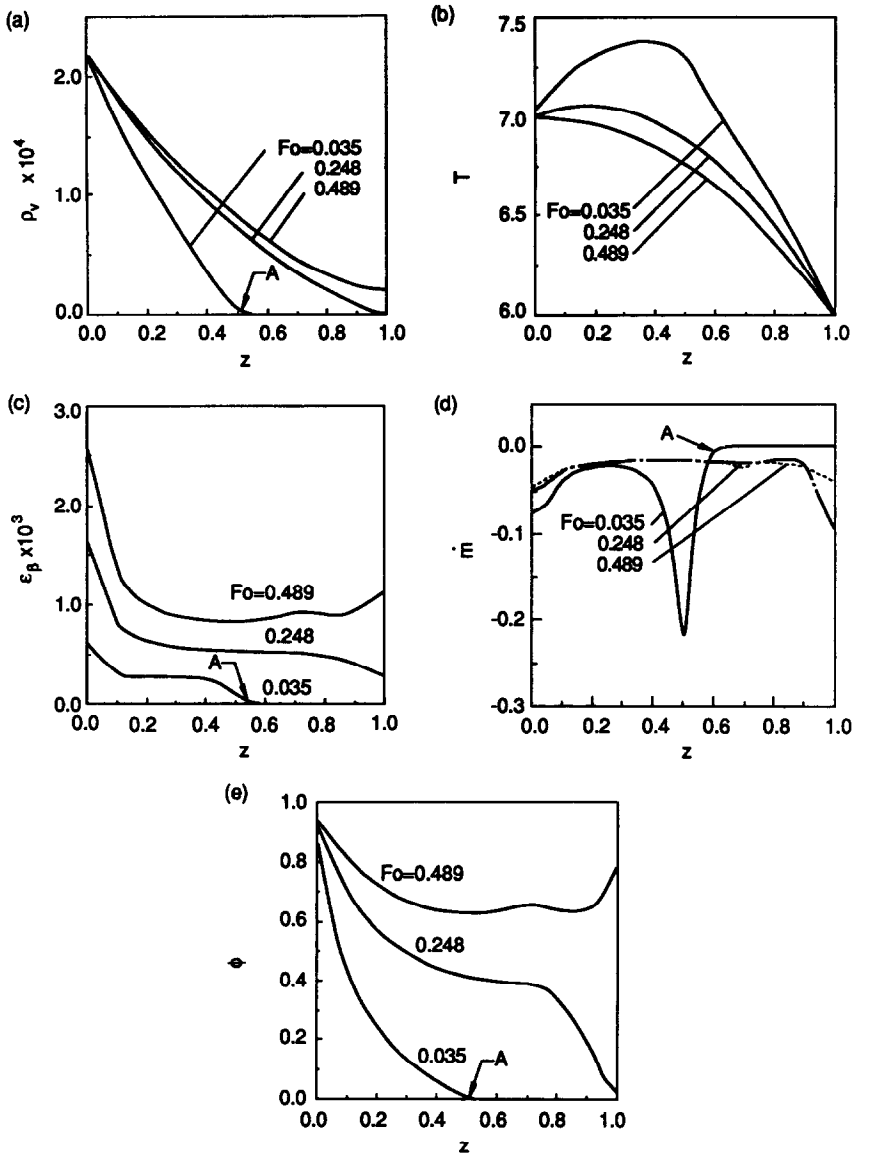

FIG. 4. Spatial distributions of: (a) ρ_v, (b) T, (c) ε_β, (d) $\dot{m}$ and (e) ϕ. $\phi_a = 0.97$, $T_c^* = 252$ K for the BET I approximation.

is near the cold side of the slab, which is different from the case using the BET I approximation. As will be discussed below, this spatial distribution in ε_β is close to the experimental observations. It should be noted that the spikes shown in the $\dot{m}$ distribution in Fig. 5(d) reflect the discontinuity in the vapor diffusion flux between different phase-change regions. Mathematically, it means the first derivative of ρ_v with respect to z is not continuous between those regions.

3.2. *Comparison of the bulk-phase-change model and experiment data*

The typical time variation of the heat flux at the cold boundary and the temperature field are shown in Figs. 6 and 7 for the cases of a closed system and an open system, where the dimensionless heat flux Q is defined as

$$Q = -k_{\text{eff}} \left.\frac{\partial T}{\partial z}\right|_{z=1}. \tag{29}$$

The results obtained from the adsorption model and the bulk-phase-change model are essentially the same for a closed system. Since there is no external vapor supply, the amount of moisture that can migrate within the slab depends entirely on the initial water vapor content. In the example shown in Fig. 6(a), $\phi_0 = 0.1$ is used which corresponds to an initial ε_β of approximately 2.6×10^{-4}, which is not small compared to the criterion set in refs. [9, 10]. Yet the tem-

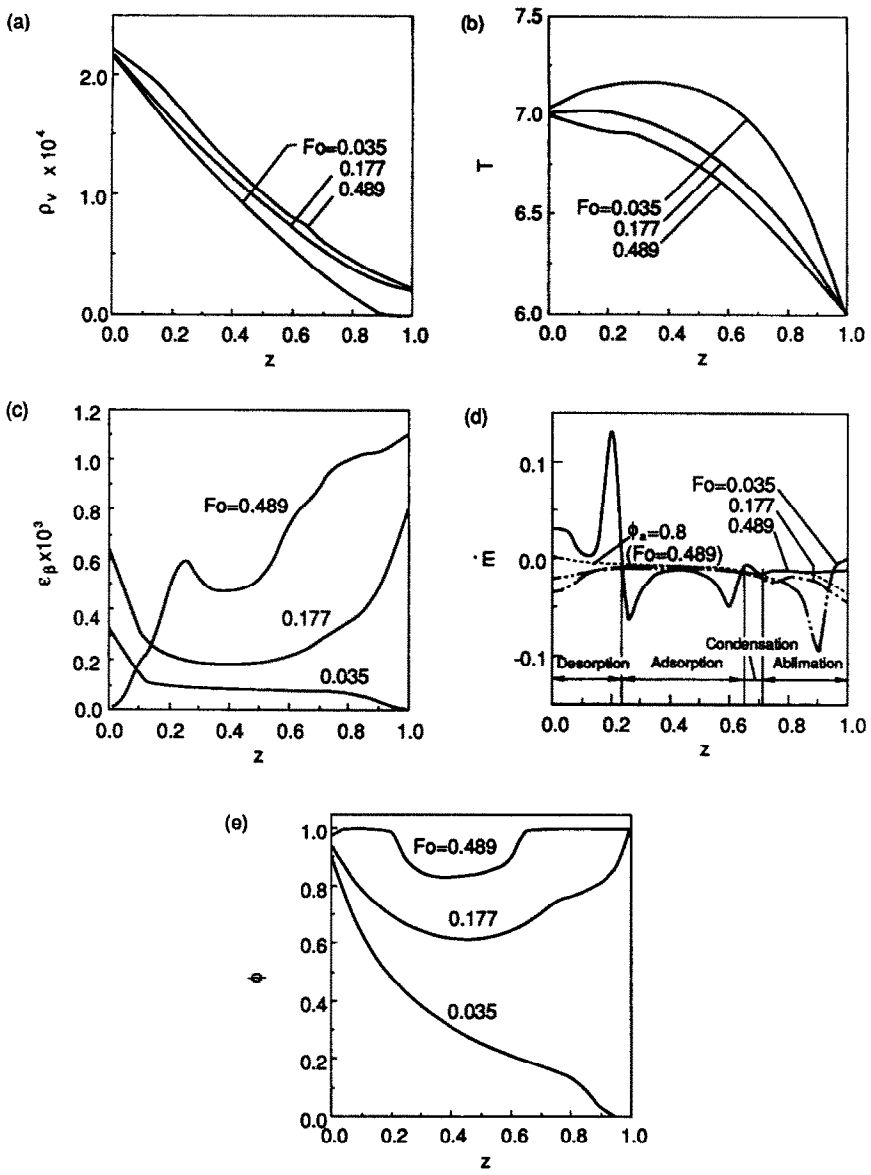

FIG. 5. Spatial distributions of: (a) ρ_v, (b) T, (c) ε_β, (d) $\dot{m}$ and (e) ϕ. $\phi_a = 0.97$, $T_c^* = 252$ K for the BET II approximation. The broken line is for $\dot{m}$ at $\phi_a = 0.80$ when $Fo = 0.489$.

perature field is not significantly influenced by the hygroscopicity of the fibers, i.e. results for the BET I approximation are very similar to the case of no hygroscopic effects (the difference between the results from the BET II approximation and from the bulk-phase-model are unnoticeable in Fig. 6(a)). This supports the experimental results for a closed system [13] in which no significant effects of hygroscopicity were shown for a medium-dry-density glass-fiber insulation. It is interesting to note that their theoretical model [13] incorrectly predicted strong effects of adsorption on a time delay for the sample reaching the steady state.

Contrary to the closed system, when the external vapor is allowed to diffuse into the slab as in an open system, the effects of hygroscopicity on the temperature field become important. As shown in Fig. 6(b), the heat flux, using the adsorption model, is higher than the prediction based on the bulk-phase-change model with no hygroscopic effects. For the adsorption model, the results for the BET I approximation (high hygroscopicity) are larger than those for the BET II approximation (low hygroscopicity). This is, of course, because of the heat source effects of phase change which increase the local temperature as seen in Fig. 7(b). The enhancement of adsorption, due to the external vapor diffusion, increases the amount of this internal heating as compared with the closed system. The alteration of the temperature field causes a time delay in reaching a quasi-steady state. From

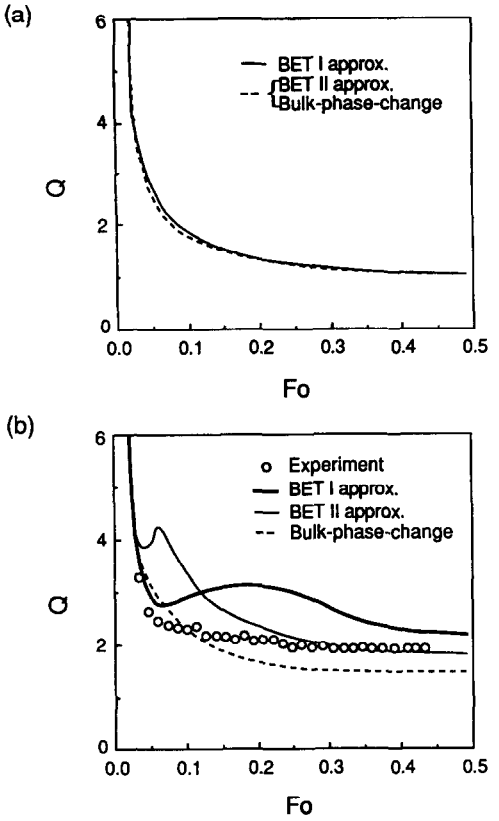

FIG. 6. Time variation of the heat flux for: (a) a closed system, $\phi_0 = 0.1$, $T_c^* = 252$ K; (b) an open system, $\phi_a = 0.80$, $T_c^* = 252$ K.

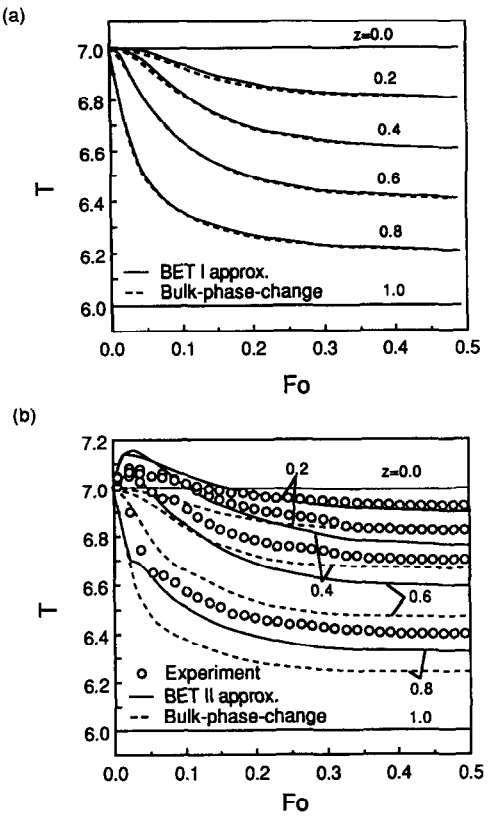

FIG. 7. Time variation of the temperature for: (a) a closed system, $\phi_0 = 0.1$, $T_c^* = 252$ K; (b) an open system, $\phi_a = 0.80$, $T_c^* = 252$ K.

Fig. 6(b), it can be seen that, according to the bulk-phase-change model, the Fourier number, at a quasi-steady state, is about 0.2, while the adsorption model predicts it to be greater than 0.33. The experimental results of the heat flux and the temperature distribution are also shown in Figs. 6 and 7. It is obvious that the experimental data agree better with the adsorption model, in spite of the uncertainties in the adsorption properties that were extrapolated for the test conditions. It is interesting to note that the quasi-steady-state values for Q and T, calculated from these two models, are different. This is because the predicted moisture accumulation from the two models is different, as can be seen from Fig. 8. The measured moisture accumulation is closer to the prediction by the adsorption model. The discrepancy in ε_β near the cold boundary ($z = 0.9$), at a sub-freezing temperature, is due to the formation of a frost layer on the cold plate of the heat-flux meter. The effect of this boundary condition on the formulation is discussed in more detail in a companion paper [19]. Putting this aside, we can then conclude that when heat and mass transfer are coupled in a transport process in porous media, which have hygroscopic effects, one cannot neglect the hygroscopic effects in predicting the temperature and heat flux. As indicated by the typical example shown in Fig. 6(b), the discrepancy in Q can

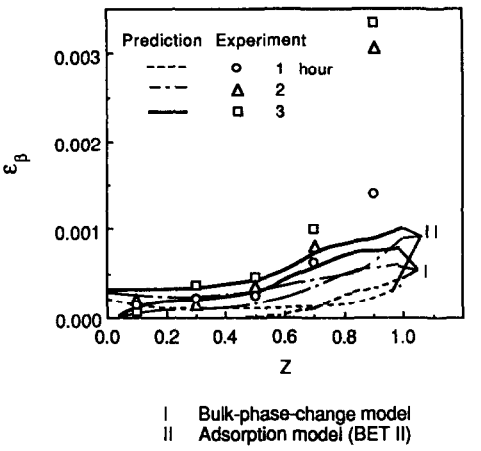

FIG. 8. Spatial distributions of ε_β obtained from the bulk-phase-change model, adsorption model and experiments.

be up to 50% at $Fo = 0.23$. Even at the quasi-steady state, it is still around 30%.

In Fig. 9, we show the influence of the ambient relative humidity and the cold temperature on a heat-flux ratio, Q', which is defined as the ratio of the heat flux, Q, to the heat flux for the same slab at a

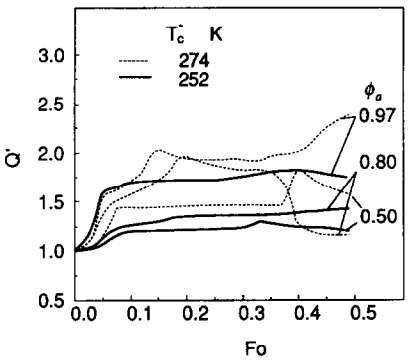

FIG. 9. Time variation of the heat flux ratio Q' for different ϕ_a and T_c^*: the open system for the BET II approximation.

completely dry condition (i.e. $\phi_a = \phi_0 = 0$) and otherwise the same initial and boundary conditions

$$Q' = \frac{\left(k_{\text{eff}} \dfrac{\partial T}{\partial z}\right)_{z=1}}{\left(k_{\text{dry}} \dfrac{\partial T}{\partial z}\right)_{z=1,\text{dry}}}. \tag{30}$$

It is shown that, compared to a dry slab, the heat loss from the cold side can be doubled due to phase changes in an open system. Also Q' is larger at a higher ϕ_a for the sub-freezing temperature. For the cold temperature above 273.16 K and for $Fo > 0.35$, the heat-flux ratio, Q', as a function of Fo, shows some abrupt changes which results in Q', at $\phi_a = 0.8$, being less than Q', at $\phi_a = 0.5$. This behavior is mainly due to the temperature variation near the cold boundary, which is influenced by the transition from physical adsorption to bulk condensation and ablimation. This transition occurs when the local relative humidity becomes greater than 0.95. As will be discussed below, the time required for a local relative humidity to reach 0.95 depends on the temperature difference across the slab and the capacity of hygroscopicity with a complex interaction among heat and mass transfer and phase change. Qualitatively, the trends, shown in Fig. 9, indicate that hygroscopicity has a stronger effect on the heat flux for the case with the cold temperature above the triple point of water than that with a sub-freezing temperature.

3.3. *A transition Fourier number qualifying the hygroscopic effects on mass transfer*

It is already shown in Figs. 6 and 7, adsorption causes a time delay in the slab reaching a quasi-steady state, especially for an open system, when the time variation of the temperature is very small (but the time variation of ε_β may not be negligible because $\dot{m}$ is not zero everywhere [12]). This time delay depends on the temperature range the insulation undergoes, the ambient relative humidity, and the hygroscopicity of the glass-fibers. A generalized, quantitative description of this relation is a complex task. However, since phase change effects associated with

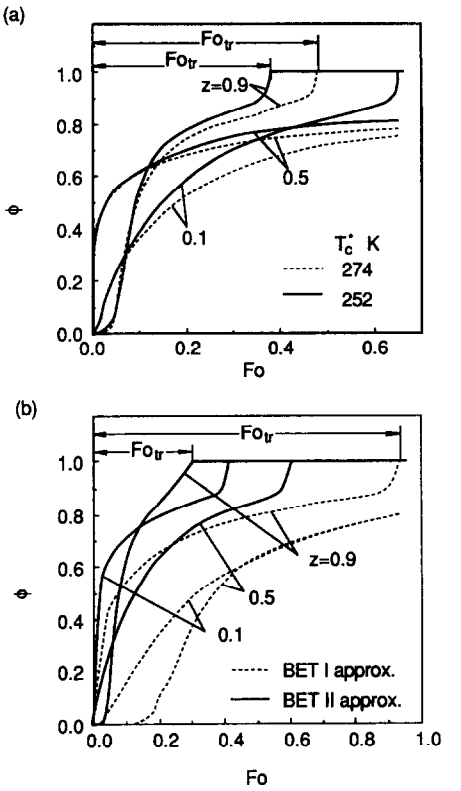

FIG. 10. The time variation of the local relative humidity for the open system: (a) the effect of T_c^*, $\phi_a = 0.97$; (b) the effect of the hygroscopic capacity, $\phi_a = 0.80$ and $T_c^* = 252$ K.

hygroscopic mass transfer is the dominating factor as we compare with the heat-transfer-only process in a dry insulation, it is reasonable to choose a mass transfer time scale as a measure of the effects of adsorption on the transient thermal response. In Fig. 10, we define a transition Fourier number Fo_{tr}, which is a dimensionless time scale, when the local relative humidity at $z = 0.9$ reaches 1.0. The reference position $z = 0.9$, chosen arbitrarily to avoid the boundary conditions at $z = 1.0$ [19], simply characterizes a finite volume of the insulation that is under the bulk phase change. The significance of Fo_{tr} is that, the larger the value of Fo_{tr}, the stronger the hygroscopic effects on the thermal response. From Fig. 10, one can see that the hygroscopic effects are more significant for a cold temperature above the triple point of water than for a sub-freezing temperature (Fig. 10(a)), and Fo_{tr} for the BET I approximation is apparently larger than that for the BET II approximation (Fig. 10(b)). At the same cold temperature ($T_c^* = 252$ K), Fo_{tr}, for $\phi_a = 0.97$ (Fig. 10(a)), is larger than that for $\phi_a = 0.8$ (Fig. 10(b)). All these results are consistent with the trends discussed above. It should be noted that the discussions here are based on a knowledge of the empirical adsorption isotherms (and the enthalpy of adsorption), which vary with the composition of the insulation (the percentage of the bonding material, dry density, etc.). Although the above qualitative con-

clusions are obvious, a quantitative relation between Q' and Fo_{tr} requires accurate, complete adsorption data which may be only achieved on a case-by-case basis. Nevertheless, the methodology presented in this study is, in principle, applicable to other hygroscopic materials.

4. SUMMARY AND CONCLUSIONS

A semi-empirical study of heat and moisture transport in a glass-fiber insulation slab is performed to include the hygroscopicity effects. Thus, in the transport processes involved, phase changes and latent heat transfer are caused by bulk condensation and frosting as well as physical adsorption and capillary condensation (hygroscopicity effects). The BET approximation, based on empirical adsorption/desorption isotherm data, is used and the relation between the enthalpy of adsorption and the amount of adsorption is also derived according to thermodynamic relations. Given the comparisons with the bulk-phase-change model and experimental results, the following conclusions may be drawn for typical glass-fiber insulations:

(a) For an initially dry glass-fiber insulation with the medium dry density, the effects of hygroscopicity on the temperature field and heat loss are negligible, if the sample is isolated from the ambient mass transfer; however, these effects are very significant when one side of the same fibrous slab is open to moist air during a transport process.

(b) For an open system, the discrepancy between the adsorption model and the bulk-phase-change model can be as high as 30% for the quasi-steady-state heat flux. The measured heat flux and temperature distribution support the adsorption model based on the BET II approximation.

(c) The effects of hygroscopicity on the transient thermal response can be characterized by a transition Fourier number which, for an open system, is larger for the insulation with a relatively high capacity of hygroscopicity, and increases as the cold temperature and the ambient relative humidity increase.

REFERENCES

1. American Society of Testing and Materials, *Water in Exterior Walls: Problems and Solutions*, ASTM STP 1107 (in press).
2. E. R. G. Eckert and M. Faghri, A general analysis of moisture migration caused by temperature differences in an unsaturated porous medium, *Int. J. Heat Mass Transfer* **23,** 1613–1623 (1980).
3. D. A. de Vries, The theory of heat and moisture transfer in porous media revisited, *Int. J. Heat Mass Transfer* **30,** 1343–1350 (1987).
4. A. P. Shapiro and S. Motakef, Unsteady heat and mass transfer with phase change in porous slabs: analytical solutions and experimental results, *Int. J. Heat Mass Transfer* **33,** 163–173 (1990).
5. C. Langlais, M. Hyrien and S. Karlsfeld, Moisture migration in fibrous insulating material under the influence of a thermal gradient. In *Moisture Migration in Buildings*, ASTM STP 779, pp. 191–206 (1982).
6. D. A. Pierce and S. M. Benner, Thermally induced hygroscopic mass transfer in a fibrous medium, *Int. J. Heat Mass Transfer* **29,** 1683–1694 (1986).
7. M. K. Kumaran, Moisture transport through glass-fibre insulation in the presence of a thermal gradient, *J. Thermal Insulation* **10,** 243–255 (1987).
8. N. E. Wijeysundera, M. N. A. Hawlader and Y. T. Tan, Water vapor diffusion and condensation in fibrous insulations, *Int. J. Heat Mass Transfer* **32,** 1865–1878 (1989).
9. K. Vafai and S. Sarker, Condensation effects in a fibrous insulation slab, *J. Heat Transfer* **108,** 667–675 (1986).
10. K. Vafai and H. C. Tien, A numerical investigation of phase change effects in porous materials, *Int. J. Heat Mass Transfer* **32,** 1261–1277 (1989).
11. H. C. Tien and K. Vafai, A synthesis of infiltration effects on an insulation matrix, *Int. J. Heat Mass Transfer* **33,** 1263–1280 (1990).
12. Y.-X. Tao, R. W. Besant and K. S. Rezkallah, Unsteady heat and mass transfer with phase change in an insulation slab: frosting effects, *Int. J. Heat Mass Transfer* **34,** 1593–1603 (1991).
13. G. P. Mitalas and M. K. Kumaran, Simultaneous heat and moisture transport through glass-fibre insulation: an investigation of the effect of hygroscopicity, *The 1987 ASME WAM-SED*, Vol. 4, pp. 1–4. ASME (1987).
14. Y.-X. Tao, R. W. Besant and K. S. Rezkallah, Heat and moisture transport through a glass-fiber slab with one side subject to a freezing temperature. In *Water in Exterior Walls: Problems and Solutions*, ASTM STP 1107 (1991) (in press).
15. F. A. L. Dullien, *Porous Media: Fluid Transport and Pore Structure*, pp. 70–71. Academic Press, New York (1979).
16. S. G. Gregg and K. S. W. Sing, *Adsorption, Surface Area and Porosity*, p. 17. Academic Press, London (1982).
17. S. Whitaker, Simultaneous heat, mass and momentum transfer in porous media: a theory of drying. In *Advanced in Heat Transfer* (Edited by J. P. Hartnett and T. F. Irvine, Jr.), Vol. 13. Academic Press, New York (1977).
18. A. V. Luikov, *Heat and Mass Transfer in Capillary-porous Bodies* (Translated by P. W. B. Harrison and Translation Edited by W. M. Pun), p. 254. Pergamon Press, Oxford (1966).
19. Y. X. Tao, R. W. Besant and K. S. Rezkallah, Modeling of frost accumulation in a fibrous insulation slab and on an adjacent cold plate, *Int. Commun. Heat Mass Transfer* **18,** 609–618.

APPENDIX A

The major assumptions made in the formulation of one-dimensional, transient heat and vapor diffusion in fibrous media, using a volume averaging technique [17] are:

(a) The total gas phase (water vapor plus air) pressure in the insulation matrix is constant.

(b) The insulation material is homogeneous and isotropic.

(c) In the insulation matrix, the solid–liquid–gas region and the solid–frost–gas region are close to local thermal equilibrium and, as a consequence, only sublimation or ablimation is considered in the frozen region.

(d) The liquid accumulation is small; therefore, it is in the pendular state.

(e) No convective gas phase flow occurs in the insulation matrix; i.e. any moisture accumulation is caused by vapor diffusion only.

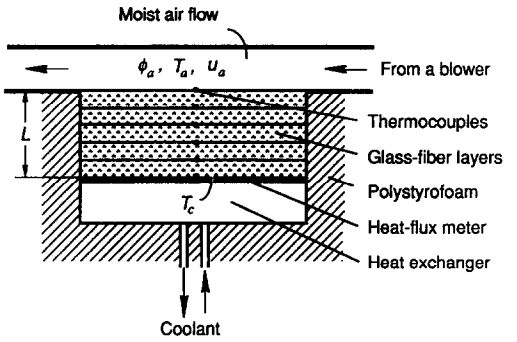

FIG. A1. A schematic of the experimental apparatus [14].

(f) In the frozen region, where the temperature is below the triple point, water is assumed to exist in the solid (ice crystal) and vapor states. The volume fraction of the ice is averaged in the local control volume with the same definition as the liquid volume fraction in the wet region. Due to the small volume fraction of ice crystal accumulation, it is assumed that frost does not exist as a self-porous medium.

(g) The temperature dependence of all the physical properties for individual phases (except gas phase density) is not considered.

Assumptions (a)–(c) have been used previously in the analysis of insulation materials [9–12]; and (d) and (e) are based on the boundary and initial conditions considered in this study. Assumption (f) is justified for small amounts of frost accumulation which is true for diffusion controlled processes. Assumption (g) emphasizes the effect of moisture/frost accumulation.

APPENDIX B

A schematic of the apparatus is shown in Fig. A1. A five-layer glass-fiber slab with a total dimension of $280 \times 600 \times 95$ mm, is placed on a cold plate which can be cooled to below the triple point temperature of water through a heat exchanger. An ethylene glycol–water solution is used as a coolant and is supplied by a pump from a storage tank which is placed in an environmental chamber. A heat-flux meter is sandwiched between the slab and the top surface of the heat exchanger to allow for the measurement of the heat flux leaving the slab. The heat-flux meter consists of a polyethylene sheet 1/8 in. (3.175 mm) thick and 21 thermocouples at each side of the sheet. An aluminum sheet, 1/8 in. (3.175 mm) thick, is mounted on the top of the polyethylene sheet to keep the surface temperature uniform and constant. The thermal conductance ($W\,m^{-2}\,K^{-1}$) of the heat-flux meter is calibrated *in situ* using a heat-flow transducer. Another 12 thermocouples are placed between the glass-fiber layers to record the temperature field of the slab. The upper surface of the slab is open to a fully developed turbulent air flow, and the other sides of the slab are covered by plastic sheets.

The glass-fiber slab is initially dried in an oven at 105°C for about 15 h and then wrapped by a plastic sheet and cooled to the room temperature. After the slab is properly mounted in the apparatus, moist air in the duct and the coolant in the heat exchanger are supplied at the same time. The air temperature and humidity and the cold temperature are stabilized within 10–15 min. The temperatures of the glass-fiber slab, air and cold plate are recorded and monitored by a microcomputer through a data acquisition unit. A typical experiment runs about 3–4 h which covers both a transient and a quasi-steady-state period. At a desired time, the slab is taken out of the apparatus and each layer is weighed using an electronic scale, to find a total amount of adsorption/moisture/frost accumulation during that period of time.

REPONSE THEORIQUE D'UNE PLAQUE ISOLANTE DE FIBRES DE VERRE AVEC EFFETS HYGROSCOPIQUES

Résumé—L'équation de Brunauer–Emmett–Teller (BET), représentant les isothermes d'adsorption, est utilisée dans un modèle monodimensionnel transitoire de diffusion de vapeur pour le transfert de chaleur et d'humidité dans une plaque isolante de fibre de verre pour tenir compte des effets hygroscopiques (adsorption de la vapeur d'eau, désorption et condensation capillaire). La correction à l'enthalpie latente de changement de phase, utilisée dans l'équation d'énergie, est dérivée d'isothermes de désorption empiriques. Les résultats obtenus pour deux types de conditions aux limites (un système clos et un système ouvert) montrent que les effets d'hygroscopicité sur la distribution de température variable sont significatifs pour une plaque avec une frontière ouverte à l'air humide: la sensitivité à l'hygroscopicité du transfert variable de chaleur et de masse peut être décrite par un nombre de Fourier qui est proportionnel à la capacité d'adsorption de la plaque et elle croît quand la température du côté froid et l'humidité relative ambiante augmentent. Etant donné l'incertitude sur les propriétés d'adsorption des fibres de verre et celle sur les données expérimentales, l'accord entre le modèle et les données est raisonnable.

DAS INSTATIONÄRE THERMISCHE VERHALTEN EINER GLASFIBER-DÄMMPLATTE UNTER BERÜCKSICHTIGUNG HYGROSKOPISCHER EINFLÜSSE

Zusammenfassung—In einem eindimensionalen instationären Dampfdiffusionsmodell für den Wärme- und Feuchtigkeitstransport in einer typischen Glasfiber-Dämmplatte mittlerer Dichte, wird zur Berücksichtigung der hygroskopischen Defekte (Wasserdampfadsorption, -desorption und Kapillarkondensation) die Brunauer–Emmett–Teller-Gleichung für die Adsorptionsisothermen verwendet. Die Korrektur der Phasenwechselenthalpie in der Energiegleichung wird aus empirischen Desorptionsisothermen abgeleitet. Die Ergebnisse für zwei Arten von Randbedingungen (geschlossenes System und offenes System) zeigen, daß die Einflüsse der Hygroskopie auf das instationäre Temperaturfeld in einer Platte bedeutsam ist, wenn eine ihrer Berandungen offen an feuchte Luft angrenzt. Der Einfluß der Hygroskopie auf den instationären Wärme-Stofftransport kann mit Hilfe einer Fourier-Zahl beschrieben werden, welche der Adsorptionskapazität der Glasfiberplatte proportional ist und mit steigender Temperatur an der kalten Seite und steigender Feuchtigkeit in der Umgebung zunimmt. Berücksichtigt man die Unsicherheit der Eigenschaften des Glasfibermaterials für Adsorption sowie der Versuchsdaten, so zeigt sich eine hinreichende Genauigkeit zwischen berechneten und gemessenen Daten.

НЕСТАЦИОНАРНЫЙ ТЕПЛОВОЙ ОТКЛИК ИЗОЛЯЦИОННОЙ ПЛАСТИНЫ ИЗ СТЕКЛОВОЛОКНА ПРИ НАЛИЧИИ ГИГРОСКОПИЧЕСКИХ ЭФФЕКТОВ

Аннотация—Уравнение Брунауэра–Эмметта–Тэллера (БЭТ), представляющее изотермы поглощения, используется в одномерной нестационарной диффузионной модели, которая описывает перенос тепла и влаги в типичной изоляционной пластине из стекловолокна с целью объяснения гигроскопических эффектов (поглощения водяного пара, десорбции и капиллярной конденсации). Коэффициент поправки к скрытой энтальпии фазового перехода, используемый в уравнении сохранения энергии, определяется по эмпирическим изотермам десорбции. Результаты, полученные при двух видах граничных условий (замкнутая и незамкнутая системы) показывают, что влияние гигроскопичности на нестационарное распределение температур является существенным в случае, когда одна граница пластины сообщается с влажным воздухом. Чувствительность гигроскопичности к неустановившемуся тепло-и массопереносу можно описать числом Фурье, значение которого пропорционально адсорбционной способности пластины из стекловолокна и возрастает по мере увеличения температуры ненагретой стороны и относительной влажности окружающей среды. При наличии неопределенности адсорбционных свойств стекловолокна и экспериментальных данных получено удовлетворительное согласие между результатами моделирования и измерений.